Scientia Iranica B (2023) 30(2), 442–453

Sharif University of Technology
Scientia Iranica
Transactions B: Mechanical Engineering
http://scientiairanica.sharif.edu

Research Note

Deformable nose design for the non-penetrating projectile

M. Taheri and O. Kavianipour*

Department of Mechanical Engineering, Damavand Branch, Islamic Azad University, Damavand, Iran.

Received 25 December 2021; received in revised form 23 June 2022; accepted 28 November 2022

KEYWORDS
Projectile;
Nose shape;
Thin-walled cylinder;
Plastic deformation;
Impact.

Abstract. This paper deals with the design of a deformable nose for the non-penetrating projectile in order to protect its body against deformation. Numerical, analytical, and experimental studies have been carried out to analyze the effect of different nose shapes on the projectile deformation when it hits the brick wall. The projectile consists of an aluminum nose, a thin-walled steel cylinder body, and an end connector. This non-penetrating projectile can be used to carry a cargo that must reach its destination safely, e.g., firefighting applications. To meet this goal, the criterion utilized for the best design in this paper is stress and strain analysis. The geometric shape of the noses includes three types: type (a), type (b), and type (c). The first type of nose is flat shape. This nose was detached from the projectile by impact and did not prevent the projectile deformation. The second type of nose was a combination of flat and conical shapes. The projectile was also deformed by this nose. The third type of nose was a combination of flat, conical, and spherical shapes. Due to the maximum absorption of the impact energy, this type of nose prevented the deformation of the cargo and projectile.

1. Introduction

1.1. General

The purpose of this research is to design a nose for a type of projectile that is used to extinguish fires in closed spaces such as stores and residential buildings. After launching and passing through an open door or window, the projectile hits the interior walls of the building (non-penetrating projectile) and then, extinguishes the fire by releasing a special gas in the closed space. The nose of this projectile should be designed such that it absorbs the impact energy and prevents the deformation of other components of the projectile. For this purpose, the plastic behavior of the walls, the geometric shape of the nose, and the plastic deformation of the projectile should be investigated.

1.2. Behavior of building materials against dynamic loads

Research has shown that the behavior of most building materials varies in dynamic and static conditions, and understanding the effects of strain rates on them is important for accurate modeling. When concrete, clay brick and mortar structures are subjected to high-velocity dynamic loads, their response parameters, damage mechanisms, and penetration depth may differ from those exposed to static forces [1–4]. Researchers have used theoretical, experimental studies, and numerical simulations to study the dynamic properties of concrete. Research results have shown that numerical simulation can provide more information about the

*. *Corresponding author.*
E-mail addresses: e.morteza.taheri@gmail.com (M. Taheri); o.kavianipour@damavandiau.ac.ir (O. Kavianipour)

doi: 10.24200/sci.2022.59623.6341

process with complex analysis; however, the data obtained from the experiment are very important [5–6]. Various studies show that the behavior of brick walls against static and dynamic loads is similar to that of concrete, which is a brittle material [7–9]. The effect of compressive strength and fracture modes of concrete and the impact velocity of the projectile on its penetration into the concrete was studied by some researchers [10–12].

1.3. Geometric shape of the projectile nose

Another important parameter for the design of this projectile is the geometric shape of the nose. It may be flat, ogival, conical, hemispherical, etc. Many researchers have studied the effect of projectile nose shape on the behavior of concrete target subjected to impact [13–16]. The effect of the geometric shape of the nose of rigid projectiles on the penetration of concrete and its residual velocity was studied by some researchers [17,18].

1.4. Deformable projectile behavior

In the above research studies, the geometric shape of the nose was investigated with a rigid projectile. In the present study, given that the firefighting projectile is deformable and its plastic behavior is important when it hits the wall of the building, the projectile is considered deformable. The study of plastic behavior of deformable projectiles when hitting brick and concrete walls has also been done by some researchers. Wang et al. [19] numerically studied the deformation of soft projectiles during impact with concrete structures. They compared numerical and laboratory results for various parameters, including the length of the damaged and remaining sections, and discussed the importance of each parameter in the shape of the projectile failure. Phillabaum et al. [20] examined the nose shape for thin-walled deformable projectiles impacting reinforced concrete numerically and experimentally. They designed two types of "spherical and ogive" noses for projectiles. The results showed that an increase in the velocity would raise the extent of projectile structure deformation after penetration into the concrete for projectiles with a spherical nose. Li and Xu [21] investigated the failure behaviors of projectiles during high-speed impact into concrete slabs. Then, they proposed a new theoretical failure model of ogive-nose projectile subjected to impact loading considering the failure mechanisms. Zhang et al. [22] theoretically studied the plastic behavior of ogival-nosed projectiles at different velocities when they impacted concrete target. By defining the velocity of the rigid body and the hydrodynamic velocity, they stated that when the impact velocity of the projectile was lower than the velocity of the rigid body, the projectile would remain in the rigid state. In addition, when its velocity was higher than the hydrodynamic velocity, the projectile would be in the erosion state; and when the velocity of the projectile was greater than and the speed of a rigid body were lower than the hydrodynamic speed, it would be in a deformable state. Liu et al. [23] studied the impact of the projectile on the concrete wall theoretically and experimentally. They observed that the strength of the projectiles and the concrete targets significantly affected the penetration depth and critical velocities. Okuda et al. [24] performed impact tests using soft projectiles to evaluate local damage to reinforced concrete. They also presented test conditions, test equipment, test results, and knowledge gained on localized damage to reinforced concrete subjected to normal and oblique impacts.

1.5. Goals of the present study

According to previous research papers, it is clear that:

1. Few studies have been performed on deformable and impenetrable projectiles within a concrete or brick wall;
2. The deformation of the projectile after hitting the target depends on various factors such as the geometric shape and material of the nose, the speed of impact, and the material and thickness of the target.

The purpose of this research is to design a deformable nose for a fire-extinguishing projectile, whose task is to transfer solid aerosol materials safely and without deformation into the fire. This research can be used to design the nose of projectiles (with various civilian and humanitarian applications) that should not be deformed such as fire extinguishing projectiles and carrier projectiles.

1.6. Description of projectile components

In this paper, the projectile consists of a thin-walled steel cylinder with one end attached to the launch engine and the other end to the nose (see Figure 1). The main objective of this work is to investigate the effect of three types of noses with the same material and different geometric shapes on the projectile deformation and to evaluate the amount of strain energy in non-penetrating conditions. One of the practical applications of this projectile is to carry a cargo that

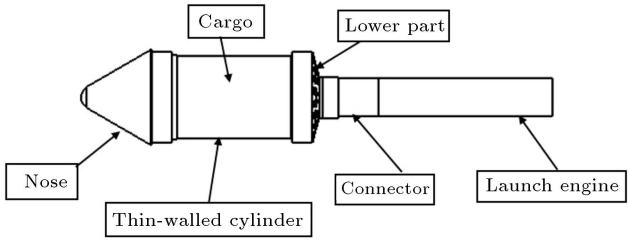

Figure 1. A schematic of the projectile.

must reach its destination safely and the thin-walled cylinder must, therefore, have the least deformation due to impact on the brick wall.

First, projectile (a) with a flat nose is considered in this research. It is shown that this nose is separated from the projectile when it hits the brick wall and cannot prevent the thin-walled cylinder deformation. Afterwards, projectiles (b_1), (b_2), and (b_3) are designed such that their geometric shapes are a combination of flat and conical noses with angles of 20, 30, and 40 degrees to the axis of the cone. It has been shown that the thin-walled cylinder deformation of these projectiles is less than that of projectile (a). Finally, projectile (c) is intended for construction, which is a combination of flat, conical (with an angle of 30 degrees to the cone axis), and spherical noses. Due to the maximum energy absorption of the projectile impact on the brick wall, this type of nose creates the least deformation for the thin-walled cylinder. It is to be noted that the launch was performed by a type of launch engine and launcher at a distance of 30 meters from the wall in all tests. Furthermore, the projectile hit the wall vertically at a speed of 50 m/s and its mass was constant and equal to 3.5 kg in all tests.

2. Simulation

ABAQUS finite element software was employed to model and simulate the projectile impact on the brick wall. Because the mentioned projectile is symmetrical, axisymmetric modeling is performed. In addition, the projectile and the brick wall are considered deformable.

2.1. Modelling of projectiles and brick walls

In this research, an explicit dynamic solution method was used to simulate the impact of the projectile on the wall. The wall was completely constrained on the one side, and the projectile velocity was only in one direction. The surface-to-surface contact was modeled for the projectile parts and the kinematic contact algorithm was considered for the wall. The effect of friction between the projectile and the wall was ignored.

The mass of all projectiles studied in this paper is 3.5 ± 0.1 kg. Given that the nose mass of the projectiles (a), (b_1), (b_2), and (b_3) is 215 ± 100 gr, the mass of the other parts of the projectile is similar to each other. However, in the projectile type (c), due to the increase in nose mass more than the mentioned range, by reducing the height of the steel cylinder and reducing the mass of cargo, the maximum mass of this projectile becomes 3.6 kg. The materials and elastic properties of the projectile, brick wall, and cargo are given in Table 1.

Many researchers have used the Johnson-Cook model to describe the plastic and failure behavior of steel and aluminum in impact problems [28]. The Johnson-Cook flow surface is defined as Eq. (1):

$$\sigma_{eq} = \left(A + B \times \varepsilon_p^n\right) \times \left(1 + C \times Ln\dot{\varepsilon}_P^*\right) \times \left(1 - \left(T^*\right)^m\right), \tag{1}$$

where:

$$\dot{\varepsilon}_P^* = \frac{\dot{\varepsilon}_P}{\dot{\varepsilon}_0}, \tag{2}$$

$$T^* = \frac{T - T_0}{T_m - T_0}. \tag{3}$$

In Eqs. (1)–(3), A, B, C, n, and m are material constants, σ_{eq} is von Mises stress, ε_p is effective plastic strain, $\dot{\varepsilon}_0$ and $\dot{\varepsilon}_P$ are base and current strain rates, respectively, T_m and T_0 are material melting temperature and room temperature, respectively, and T is the actual temperature of the materials during dynamic loading.

The Johnson-Cook dynamic failure model is defined as Eq. (4):

Table 1. Materials and elastic properties of the projectile [25] and [26], brick wall, and cargo [27].

Component	Material	Density (kg/m^3)	Poisson's ratio	Young's modulus (GPa)
Nose type (a)	Al2024-T3	2700	0.33	73.8
Nose type (b_1)	Al2024-T3	2700	0.33	73.8
Nose type (b_2)	Al2024-T3	2700	0.33	73.8
Nose type (b_3)	Al2024-T3	2700	0.33	73.8
Nose type (c)	Al2024-T3	2700	0.33	73.8
Thin-walled cylinder	CK45	7800	0.3	210
Lower part	CK45	7800	0.3	210
Connector	Al2024-T3	2700	0.33	73.8
Target	Masonry wall	1887	0.2	18
Cargo	Masonry materials	1887	0.2	18

Table 2. Properties of plastic and failure for CK45 steel [31] and [32] and aluminum AL2024-T3 [33].

Johnson-Cook parameters	AL 2024-T3	CK45
A (MPa)	369	553
B (MPa)	684	600
C	0.0083	0.013
N	0.73	0.234
M	1.7	1
T_m (k)	775	1733
T_0 (k)	350	350
D_1	0.112	0.25
D_2	0.123	4.38
D_3	1.500	2.68
D_4	0.007	0.002
D_5	0.0	0.61

$$\varepsilon_f = \left[D_1 + D_2 \exp\left(D_3\left(\frac{\sigma_{me}}{\sigma_{eq}}\right)\right)\right] \times \left(1 + D_4 \times Ln\dot{\varepsilon}_p^*\right) \times \left(1 + D_5 T^*\right), \quad (4)$$

where ε_f is fracture strain, D_1 to D_5 are the damage model constants, and σ_{me} is the mean stress. The parameters of Eqs. (1) and (4) for the materials used in this paper are given in Table 2.

Generally, in finite element ABAQUS software, three methods are suggested to model the nonlinear behavior of concrete, i.e., discrete cracking model, smeared cracking model, and concrete damage plasticity model. Concrete damage plasticity material model is one of the most common constitutive models to simulate the nonlinear behavior of brittle materials such as concrete [29,30].

Due to the correspondence of numerical results in the application of the damaged plasticity model in ABAQUS software for brick walls with experimental results in [29], the damaged plasticity model was employed to model the plastic behavior of brick walls in this work.

In Table 3, σ_y is yield stress, F_{b0}/f_{c0} is maximum two-axis to single-axis compressive stress ratio, and K is the second constant ratio of the stress tensor on the tensile meridian to the same parameter on the pressure meridian. The dilation angle determines the amount of lift due to shear displacement. Actually, this phenomenon is the effect of surface roughness that is manifested in this way. The eccentricity cuts off the flow potential function at the beginning of the horizontal axis of the hydrostatic stress at an angle of 90 degrees. In fact, the function will be a curve under that condition [34].

The numerical simulations for the projectile and wall have been performed using axisymmetric mesh. The wall and projectile have been meshed with CAX4R elements corresponding to four nodes and reduced integration [35]. The optimal mesh has been obtained using a convergence method (stability of the results without mesh dependency). The wall has been meshed with 800 elements, and projectiles have been meshed with 3865 elements for the projectile (a), 2916 elements for the projectile (b_1), 2884 elements for the projectile (b_2), 2873 elements for the projectile (b_3), and 3615 elements for the projectile (c), respectively. The contact between the projectile and the wall has been defined by means of a penalty contact algorithm and a hard contact model, both of them available in ABAQUS-explicit. The "hard contact" option allows adjusting automatically the stiffness generated by the "penalty contact algorithm" in order to minimize penetration without adversely affecting the time increment. The so-called Lagrangian adaptive meshing was utilized in the impact region of the target directly in front of the projectile. Adaptive meshing is highly significant in the problem of large deformations because it provides a faster and more accurate solution than pure Lagrangian analysis.

To model the projectile in this paper, five different types of noses are considered. In other words, the geometric shape of the nose for projectile (a) is flat; projectile (b) is a combination of conical and flat shapes; and projectile (c) is a combination of conical, flat, and spherical shapes (see Figure 2).

2.2. Simulation results

For the simulation, the projectile strikes the wall at a speed of 50 m/s and is deformed, as shown in Figure 3. The simulation results reveal that the geometric shape of the projectile nose has a significant effect on its deformation when it hits the wall. The dynamic progressive buckling results in folds that generally occur at the end of the thin-walled cylinder. These folds appear in the end that are near the wall. This type of buckling is created according to the geometry of the thin-walled cylinder, loading conditions, and material properties [36].

Table 3. Characteristics of the plastic behavior of brick wall and cargo [34].

Material	σ_y (MPa)	Dilation angle	Eccentricity	F_{b0}/f_{c0}	K	Viscosity parameter
Wall	21.73	7	0.1	1.16	0.66	0.0005
Cargo	21.73	7	0.1	1.16	0.66	0.0005

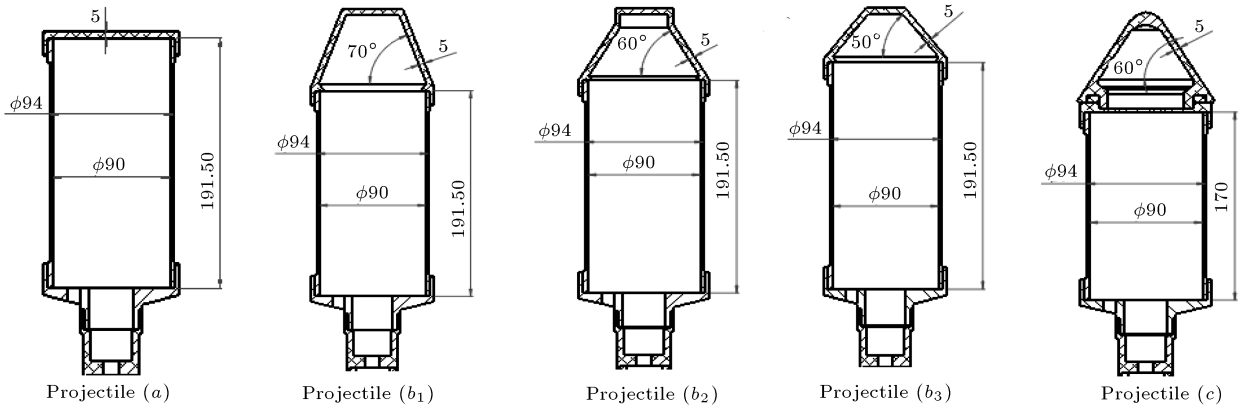

Figure 2. Five different types of projectiles considered in this paper.

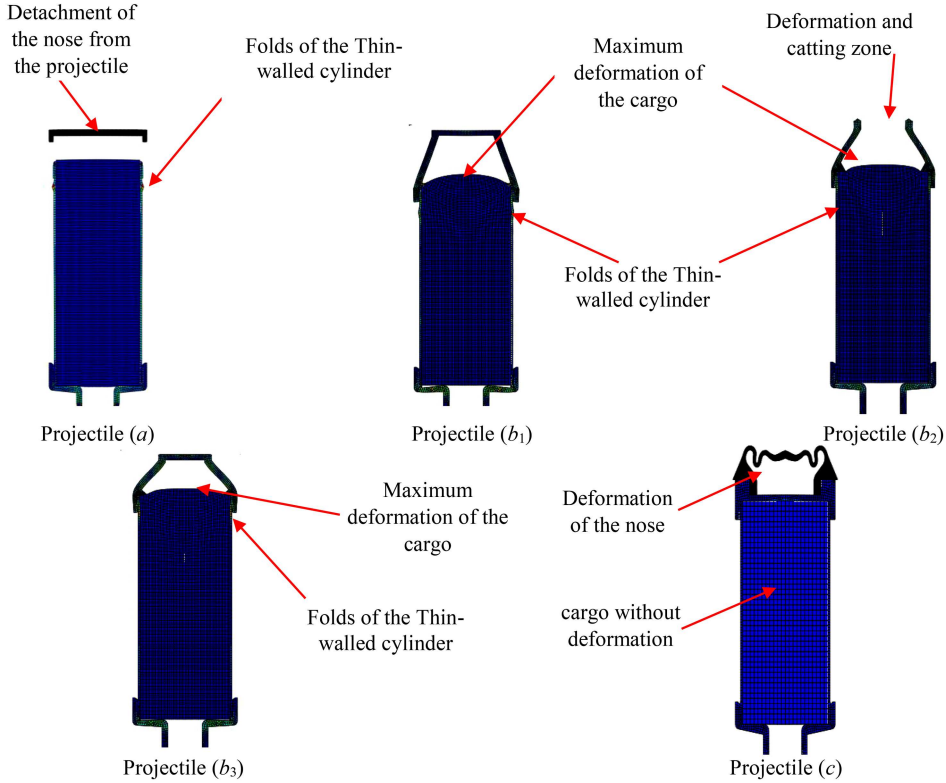

Figure 3. Deformation of the projectile after hitting the brick wall in ABAQUS software.

As seen in Figure 3, the nose of the projectile (a) is deformed and detached from the projectile and the steel cylinder undergoes large deformation after hitting the brick wall. The nose of the projectile (b_2) is broken in the flat part and, in turn, causes this part to separate from the nose. Moreover, the cargo in the steel cylinder of the projectiles (b_1), (b_2), and (b_3) is deformed. Although spherical and conical noses are deformed in projectile (c), no deformation is observed in the flat nose and the projectile and its cargo are not deformed.

By calculating the von Mises stress of the projectile during the impact on the brick wall as shown in Figure 4, the maximum stresses of the thin-walled steel cylinder in projectiles (a), (b_1), (b_2), (b_3), and (c) are 637.56 MPa, 846.67 MPa, 556.63 MPa, 822.42 MPa, and 130.52 MPa, respectively. By comparing those values with the yield stress of the steel cylinder (i.e., 553 MPa), it is found that the stress of the steel cylinder in projectile (c) is less than its yield stress. Conversely, the stress of the steel cylinder in other projectiles is greater than the yield stress of the steel cylinder.

The noteworthy point in this figure is that the stress of the steel cylinder in projectiles (b_1) and (b_3) is maximized in an infinitesimal time. It should be noted that the steel cylinder stress of projectiles (b_1) and (b_3) is higher than that of projectile (b_2). For this

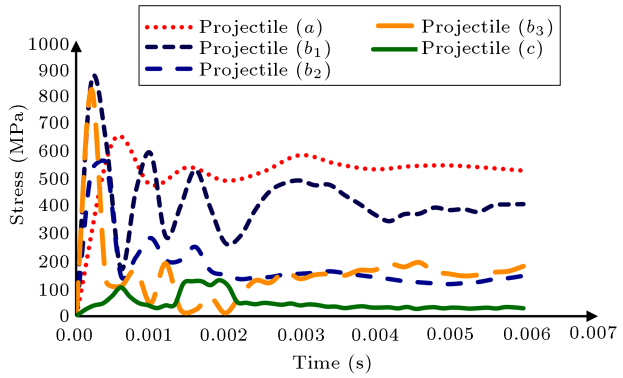

Figure 4. Von Mises stress of the thin-walled steel cylinder.

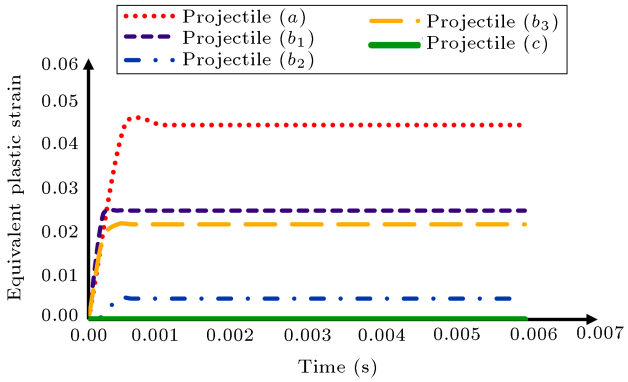

Figure 5. Equivalent plastic strain of the thin-walled steel cylinder.

reason, projectiles (b_1) and (b_3) are not considered in experimental tests in this paper.

By calculating the equivalent plastic strain of the thin-walled steel cylinder, it is revealed that the geometric shape of the nose has a substantial effect on the strain of the projectile (see Figure 5).

Figure 5 illustrates that the maximum equivalent plastic strain of the steel cylinder in projectiles (a), (b_1), (b_2), (b_3), and (c) is 0.045, 0.025, 0.005, 0.022, and 0, respectively. This figure also demonstrates that the nose shape in projectile (a) causes the most plastic strain, while the nose shape in projectile (c) creates the least plastic strain in the thin-walled steel cylinder. As shown in Figure 5, the angle of the nose shape (b_2) is optimal compared to those of nose shapes (b_1) and (b_3) to minimize the amount of plastic strain.

3. Stress analysis

Using analytical relations, the axial stress applied to the thin-walled cylinder of projectile (a) can be calculated. In this regard, there are simplistic assumptions that reduce the accuracy of the results. When two deformable objects collide with each other, one object can be considered rigid while the other deformable in order to simplify the analysis.

3.1. Rigid wall

If it is assumed that the wall is rigid and the projectile is deformable, Eqs. (5) and (6) are proposed to calculate the axial stress applied to an inelastic projectile with flat nose when striking a rigid wall [37]:

$$\sigma_m = F_Y + V_0 \left(\rho \times C_{pL}\right), \tag{5}$$

$$C_{PL} = \sqrt{\frac{E_P}{\rho}}, \tag{6}$$

where σ_m is the axial stress applied from the wall to the projectile; F_Y is the yield stress of the projectile; V_0 is the speed of the projectile hitting the wall; ρ is the density of the projectile; C_{PL} is the wave propagation velocity in the plastic range; and E_p is the plastic modulus. By considering the Johnson-Cook model to describe the plastic behavior of projectile and comparing Eqs. (1) and (5), it is clear that:

$$F_Y = A, \tag{7}$$

and according to [37]:

$$E_P = B. \tag{8}$$

By applying Eqs. (7) and (8), substituting the values of the parameters in Eqs. (5) to (8) from Tables 1 and 2, and assuming $V_0 = 50$ m/s, the axial stress applied from the wall to the projectile can be calculated as follows:

$$\sigma_m = 661 \text{ MPa}.$$

3.2. Rigid projectile

To calculate the stress applied from the wall to the projectile, Moxley et al. [38] considered the projectile to be rigid and the target to be deformable. By means of the energy method, they proposed Eqs. (9) and (10) to estimate the average force and axial stress applied to the projectile when hitting the target:

$$\sigma_{axial} = \frac{F_{AVE}}{A_a}, \tag{9}$$

$$F_{AVE} = \frac{W V_0^2}{2gP}, \tag{10}$$

where W is the weight of the projectile, P is the maximum depth of penetration, g is the acceleration due to gravity, σ_{axial} is the axial stress, and A_a is the thin-walled cylinder cross section area. Utilizing the experimental results in this research, the approximate amount of projectile penetration into the brick wall is 11 mm. Considering the values of the parameters in Tables 1 and 2 and assuming $V_0 = 50$ m/s, $W = 3.5$ g, the axial stress applied from the brick wall to the projectile is equal to 688 MPa.

Table 4. Comparison of analytical and numerical results for axial stress applied to the projectile (a).

Maximum axial stress by numerical method (MPa)	Axial stress by analytical method (MPa)	Error (%)
637.56	661 using Eq. (5)	3.7
637.56	688 using Eq. (9)	7.9

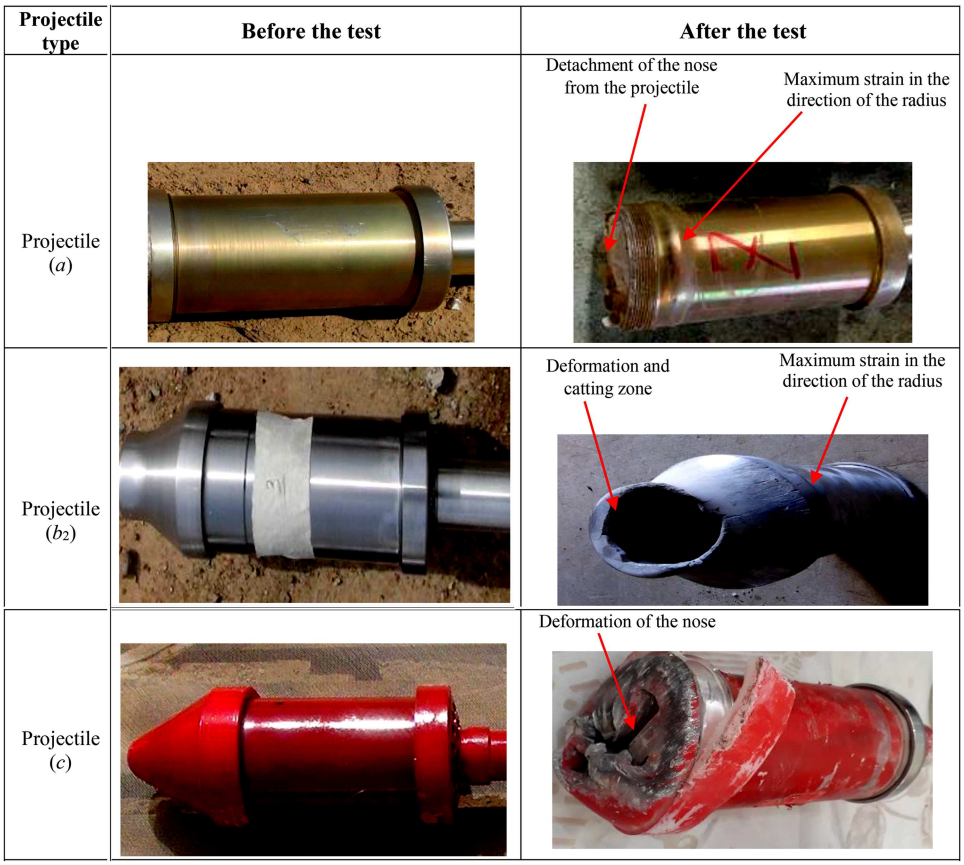

Figure 6. Projectiles before and after hitting the brick wall.

Comparing the results of analytical and numerical methods in Table 4, it is clear that there is a little difference between those results due to simplifying assumptions. This comparison also reveals that the analytical method of [37] is more accurate than that proposed in [38].

The stress applied to the thin-walled cylinder in analytical methods is estimated to be higher than the numerical method, because some of the impact energy used in the numerical and analytical methods to deform the wall and nose, respectively, due to their rigidity is directed at increasing the stress on the thin-walled cylinder.

4. Experimental test

To perform the practical experiment, three projectiles (a), (b_2), and (c) were made and steel cylinders were filled with similar cargo. The nose of projectiles and the connectors were made of 2024-T3 aluminum and the material of the lower part was CK45. The projectile was fired horizontally at a speed of 50 m/s and a distance of 30 meters from the wall.

Figure 6 shows the projectiles before and after hitting the brick wall. In this figure, it is clear that the nose of projectile (a) is detached from the projectile after hitting the wall and the thin-walled steel cylinder has been significantly deformed due to the impact on the brick wall. When projectile (b_2) hit the brick wall, the thin-walled steel cylinder was slightly deformed and the tip of the nose was broken. Generally, the nose of projectile (b_2) absorbs more energy than that of projectile (a) when the projectile hits the brick wall. The nose shape of projectile (c) is a combination of flat, conical, and spherical shapes. After assembling this type of the nose on a thin-walled steel cylinder, the projectile is fired into the brick wall as in previous experiments. It is observed that the nose of this

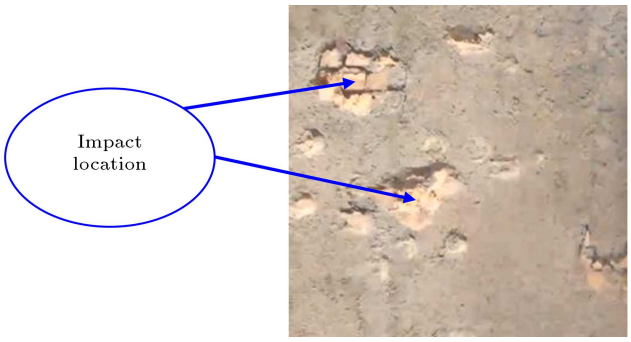

Figure 7. Brick wall impacted by the projectiles.

projectile absorbs the most impact energy compared to the previous two cases and causes the least deformation in the case of the steel cylinder.

Due to the severe impact on the projectile and the impossibility of dismantling it after the impact, the internal condition of the cargo is not visible. However, due to the proper performance of cargo after colliding and extinguishing a closed space fire, it is possible to ensure its safety and non-deformation and the accuracy of the simulation, consequently.

According to the results shown in Figure 6, it is obvious that the deformation of the projectiles after hitting the brick wall in experimental tests is quite similar to the numerical results shown in Figure 3.

Figure 7 shows the brick wall impacted by the projectiles. In this figure, it is clear that the destruction of the wall due to the projectile was superficial and it did not receive much damage.

5. Comparison between simulation results and practical tests

The maximum strain of the thin-walled steel cylinder in the direction of cylinder radius is shown in Figure 8. Figure 8 demonstrates that the maximum true strain of the steel cylinder in projectiles (a), (b_2), and (c) is 0.033, 0.0046, and 0, respectively. These strains cause the outer diameter of the cylindrical shell in projectiles (a) and (b_2) to change into 95.54 mm and 94.22 mm, respectively. For projectile (c), the outer diameter of the cylindrical shell remains unchanged.

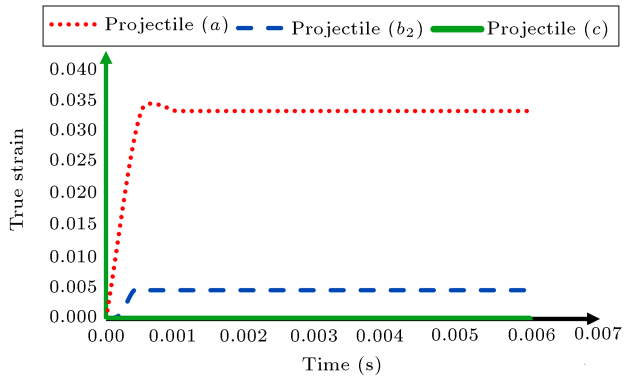

Figure 8. Radial strain of the thin-walled steel cylinders in projectiles (a), (b_2), and (c).

In order to ensure the correctness of the maximum deformation of thin-walled steel cylinders for different nose shapes, the simulation results using ABAQUS software are compared with the practical results by means of the test. A comparison of cylindrical shell diameters before and after the impact on the wall is given in Table 5. As shown in this table for three steel cylinders with an outer diameter of 94 mm before the impact, the discrepancy of the maximum outer diameter after the impact between the simulation and experimental results for projectiles (a), (b_2), and (c) is 0.66%, 0.87%, and 0.49%, respectively. Consequently, it is found that the simulation results are remarkably consistent with the experimental results.

6. Results and discussion

After numerical simulations and practical tests, the important role of the nose in the stress and strain of the projectile and the amount of strain energy absorbed by the projectile can be comprehended. In other words, a change to the geometry of the nose can alter the amount of stress and strain of the projectile.

6.1. Stress

One of the key factors in the deformation of the thin-walled steel cylinder is the amount of stress due to impact on the wall. Von Mises stress of steel cylinders

Table 5. A comparison of cylindrical shell diameters before and after the impact on the wall.

Type of projectile	Outer diameter before the collision (mm)	Maximum outer diameter of the cylindrical shell after the collision using the numerical method (mm)	Maximum outer diameter of the cylindrical shell after the collision using the practical test (mm)	Error (%)
(a)	94	95.54	96.17	0.66
(b_2)	94	94.22	95.04	0.87
(c)	94	94	94.46	0.49

in different projectiles was calculated and shown in Figure 4. This figure reveals that:

1. The stress of steel cylinders does not have a constant value at the initial moments of collision. After a few oscillations in a very short time, it remains unchanged;
2. Comparing the maximum stress of the steel cylinders, it is observed that the maximum stresses of projectiles (b_1) and (c) are the highest and lowest values, respectively;
3. The stress of the steel cylinder in projectile (b_1) reaches its maximum value, 846.67 MPa, within 0.0002 seconds;
4. The stress of the steel cylinder in projectile (c) reaches its maximum value, 130.52 MPa, within 0.0019 seconds;
5. After 0.0005 seconds, the stresses of projectile (a) are maximum values.

6.2. Energy

According to Figure 9, the maximum strain energy of projectiles (a), (b_2), and (c) is 543.7 J, 356.4 J, and 124.4 J, respectively. This energy has initially a positive value and after a while, except for the projectile (c), it acquires a negative value. The reason for the positive energy at the beginning of the collision is that the stress and strain are both in the same direction at the time interval.

The impact duration of projectiles (a) and (b_2) on the wall is shorter than that of projectile (c). After separating from the wall, the related stress is removed and the resulting stress wave remains in the projectile. On the other hand, the deformation continues due to the inertia force of the launch engine. This leads to the stress and strain in the opposite direction and in, turn, causes the negative strain energy.

The strain energy in the projectile (c) is not negative because of the special geometric shape of the nose. It plays an important role in increasing the duration of impact and energy absorption. Moreover, this type of the nose considerably diminishes the effect of the inertia force of the launch engine during the impact. Subsequently, the stress due to the inertia force of the engine is less than the stress generated by the resulting stress wave.

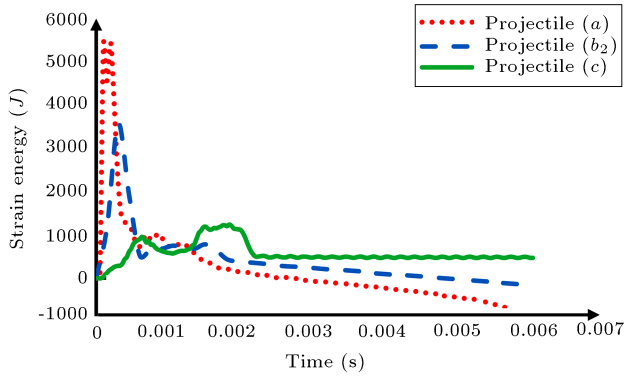

Figure 9. A comparison of strain energy of projectiles (a), (b_2), and (c).

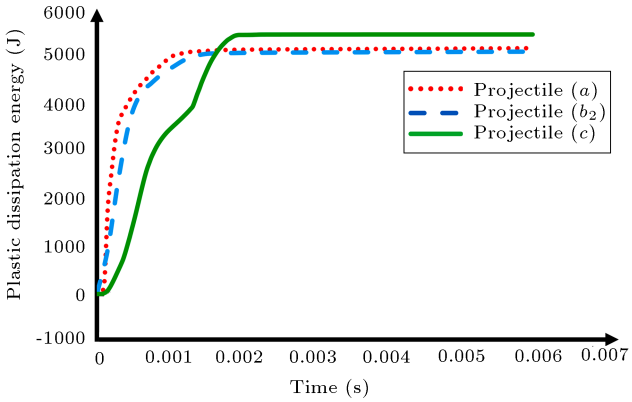

Figure 10. A Comparison of plastic dissipation energy of projectiles (a), (b_2), and (c).

As shown in Figure 10, the maximum plastic dissipation energy of projectiles (a), (b_2), and (c) is 5167 J, 5093.6 J, and 5457.9 J, respectively. Both numerical results and experimental tests demonstrate that no plastic deformation occurred in the components of projectile (c) except its nose. Hence, it can be said that the plastic dissipation energy in the projectile (c) is approximately absorbed by the nose. Actually, the nose of projectile (c) absorbs the most energy due to its design and causes more plastic dissipation energy than the other two types. Therefore, the nose of projectile (c) can prevent the thin-walled cylinder from deforming.

7. Conclusion

In this paper, the design of a deformable nose for the non-penetrating projectile was studied.

Actually, the plastic behavior of projectiles with different nose shapes and the effect of the three noses on the deformation of the projectile due to the impact on the brick wall were investigated numerically and experimentally. The projectile was comprised of a thin-walled steel cylinder with one end attached to the launch engine and the other end to an aluminum nose. Numerical analysis of the projectile impact on the wall in non-penetrating conditions was performed by ABAQUS finite element software. Afterward, experimental tests confirmed the accuracy of the numerical results.

The purpose of this research was to design a deformable nose for a fire extinguishing projectile, whose task is to transfer solid aerosol materials safely and without deformation into the fire. This research

can be used to design the nose of projectiles (with various civilian and humanitarian applications) that should not be deformed, such as fire extinguishing projectiles and carrier projectiles. Therefore, the thin-walled cylinder must have the least deformation due to impact on the brick wall. It was observed that the nose of projectile (c) could prevent the thin-walled cylinder from deforming.

The third type of nose in this paper, type (c), was a combination of flat, conical (with an angle of 30 degrees to the cone axis), and spherical noses. The simulation results revealed that the maximum von Mises stress and the maximum equivalent plastic strain of the thin-walled steel cylinder in projectile (c) during the impact on the brick wall were 130.52 MPa (less than its yield stress, i.e., 553 MPa) and 0, respectively. Experimental tests clarified that the discrepancy of the maximum outer diameter of the steel cylinder after the impact between the simulation and experimental results for projectile (c) was 0.49%. Hence, the simulation results are remarkably consistent with the experimental results. It was shown that the impact duration for projectile (c) is longer than the other two cases and the nose of projectile (c) absorbs the most energy from hitting the wall. As a result, the thin-walled cylinder in the projectile (c) has the least deformation due to collision with the brick wall.

Nomenclature

A, B, C	Material constants
A_a	Thin-walled cylinder cross section area
C_{PL}	Wave propagation velocity in the plastic range
$D_1 - D_5$	Material constants
E_P	Plastic modulus
F_Y	Yield stress of the projectile
F_{b0}/f_{c0}	Maximum two-axis to single-axis compressive stress ratio
g	Acceleration due to gravity
K	Second constant ratio of the stress tensor on the tensile meridian to the same parameter on the pressure meridian
m	Temperature sensitivity
n	Strain hardening exponent
P	Maximum depth of penetration
T	Current temperature
T_0	Room temperature
T_m	Melting temperature
V_0	Speed of the projectile hitting the wall
W	Weight of the projectile
ε_f	Fracture strain
ε_p	Plastic strain
$\dot{\varepsilon}_P$	Plastic strain rate
$\dot{\varepsilon}$	Strain rate
$\dot{\varepsilon}_0$	Base strain rates
ρ	Density of the projectile
σ_{axial}	Axial stress
σ_{eq}	Von Mises stress
σ_m	Axial stress applied from the wall to the projectile
σ_{me}	Mean stress
σ_y	Yield stress

References

1. Hao, H. and Tarasov, B. "Experimental study of dynamic material properties of clay brick and mortar at different strain rates", *Aust J. Struct Eng*, **8**(2), pp. 117–132 (2008).
2. Yankelevsky, D.Z., Feldgun, V.R., and Karinski, Y.S. "Concrete target quasi-static resistance to a penetrating projectile considering the material constitutive relationships", *International Journal of Impact Engineering*, **156**, pp. 3–13 (2021).
3. Huang, H., Chuanlong, Z., Zhijun, L., et al. "Analysis of mechanical haracteristics of walls of masonry structure house under dynamic load", *4th International Conference on Civil, Architecture and Environment Research*, pp. 1–7 (2021).
4. Beppu, M., Shinnosuke Kataoka, S., Mori, K., et al. "Local damage characteristics of reinforced concrete slabs subjected to hard/deformable projectile impact", *Advances in Structural Engineering*, **25**(7), pp. 1505–1518 (2022).
5. Nguyen, X.B. and Nguyen, T.T. "Using the simplified concrete damage plasticity model in studying the penetration depth in concrete", *Defect and Diffusion Forum*, **415**, pp. 109–114 (2022).
6. Han, P., Liu, J., Fei, B., et al. "A study on steel-concrete-steel wall to resist perforation from rigid projectile impact", *Shock and Vibration*, **2021**, Article ID 9986062, pp. 1–12 (2021).
7. Asad, M., Zahra, T., and Thambiratnam, D. "Failure of masonry walls under high velocity impact – A numerical study", *Engineering Structures*, **238**, pp. 1–16 (2021).
8. Wang, C., Chen, A., Li, Z., et al. "Experimental and numerical investigation on penetration of clay masonry by small high-speed projectile", *Defence Technology*, **17**, pp. 1514–1530 (2021).
9. Rosenberg, Z. and Vayig, Y. "The scaling issue in the penetration of concrete targets by rigid projectiles – Revisited", *International Journal of Impact Engineering*, **140**, pp. 1–7 (2020).

10. Xu, X., Ma, T., and Nin, J. "Failure mechanism of reinforced concrete subjected to projectile impact loading", *Engineering Failure Analysis*, **96**, pp. 468–483 (2019).

11. Zhang, F., Poh, L.H., and Zhang, M. "Resistance of cement-based materials against high-velocity small caliber deformable projectile impact", *International Journal of Impact Engineering*, **144**, pp. 1–24 (2020).

12. Xu, X., Ma, T., and Ning, T. "Failure analytical model of reinforced concrete slab under impact Loading", *Construction and Building Materials*, **223**, pp. 679–691 (2019).

13. Yankelevsky, D. and Feldgun, V. "The embedment of a high velocity rigid ogive nose projectile into a concrete target", *International Journal of Impact Engineering*, **144**, pp.1–15 (2020).

14. Xu, L.Y., Xu, H., and Wen, H.M. "On the penetration and perforation of concrete targets struck transversely by ogival-nosed projectiles – a Numerical study", *International Journal of Impact Engineering*, **125**, pp. 39–55 (2019).

15. Liu, J., Li, J., Fang, J., et al. "Ultra-high performance concrete targets against high velocity projectile impact – a-state-of-the-art review", *International Journal of Impact Engineering*, **160**, p. 104080 (2022).

16. Kang, Z., Nishida, A., Okuda, Y., et al. "Impact simulations on local damage of reinforced concrete panel influenced by projectile nose shape", *Mechanical Engineering Journal*, **3**, pp. 1–13 (2020).

17. Cho, H., Choi, M.K., Park, S., et al. "Determination of critical ricochet conditions for oblique impact of ogive-nosed projectiles on concrete targets using semi-empirical model", *International Journal of Impact Engineering*, **165**, p. 104214 (2022).

18. Zakir, S.M., Tao, S., Yulong, L., et al. "Numerical studies of penetration in light armor, Concrete and Brick-Wall Targets", *Matéria (Rio J.)*, **23**(3), pp. 1–15 (2018).

19. Wang, F., Liu, J., Wang, X., et al. "Finite element analyses on the soft projectile impact testing of a wall-floor-wall reinforced concrete structure", *International Conference on Artificial Intelligence and Advanced Manufacturing*, pp. 1–10 (2019).

20. Phillabaum, R.A., Schraml, S., Summers, R., et al. "Consideration of nose shape for thin-walled projectile penetrating double reinforced concrete", *12th International Symposium on Interaction of the Effects of Munitions with Structures*, New Orleans, LA. (2005).

21. Li, Z. and Xu, X. "Theoretical investigation on failure behavior of ogive-nose projectile subjected to impact loading", *Materials*, **5372**(13), pp. 1–19 (2020).

22. Zhang, Y.D., Lu, Z.C., and Wen, H.M. "On the penetration of semi-infinite concrete targets by ogival-nosed projectiles at different velocities", *International Journal of Impact Engineering*, **129**, pp. 128–140 (2019).

23. Liu, C., Zhang, X.F., and Chen, H.H. "Experimental and theoretical study on steel long-rod projectile penetration into concrete targets with elevated impact velocities", *International Journal of Impact Engineering*, **138**, pp. 305–317 (2020).

24. Okuda, Y., Nishida, A., Kang, Z., et al. "Experimental study on local damage to reinforced concrete panels subjected to oblique impact by projectiles", *Journal of Nuclear Engineering and Radiation Science*, **9**(2), pp. 1–12 (2022).

25. Yari, R., Zarepour, H., and Ghassemi, A. "Empirical and numerical study of gas turbine disks under mechanical stress and temperature gradient", *Journal of Modern Processes in Manufacturing and Production*, **8**(2), pp. 57–72 (2019).

26. Jamal-Omidi, M. and Mohammadi Suki, M.R. "A numerical study on aluminum plate response under low velocity impact", *Ije Transactions, Aspects*, **30**(3), pp. 440-448 (2017).

27. Akhaveissy, A.H. and Desai, C.S. "Unreinforced masonry walls – Nonlinear finite element analysis with a unified constitutive model", *Arch Comput Methods Eng.*, **18**, pp. 485–502 (2011).

28. Kpenyigba, K.M., Jankowiak, T., Rusinek, A., et al. "Influence of projectile shape on dynamic behavior of steel sheet subjected to impact and perforation", *Thin-Walled Structures Elsevier*, **65**, pp. 93–104 (2013).

29. Dehghan, S.M., Najafgholipour, M.A., Kamrava, A.R., et al. "Application of ordinary fiber-reinforced concrete layer in in-plane retrofitting of unreinforced masonry walls – Test and modeling", *Scientia Iranica Journal*, **26**(3), pp. 1089–1103 (2019).

30. Anas, S.M., Alam, M., and Umair, M. "Air-blast response of axially loaded clay brick masonry walls with and without reinforced concrete core", *Advances in Structural Mechanics and Applications*, pp. 39–57 (2021).

31. Devotta, A.M., Sivaprasad, P.V., Beno, T., et al. "A modified johnson-cook model for ferritic-pearlitic steel in dynamic strain aging regime", *Metals*, **9**, p. 528 (2019).

32. Murugesan, M. and Jung, D.W. "Johnson-Cook material and failure model parameters estimation of AISI-1045 medium carbon steel for metal forming applications", *Materials*, **12**, p. 609 (2019).

33. Kay, G. "Failure modeling of titanium 6Al-4V and aluminum 2024-T3 with the Johnson-Cook material model", FAA Report DOT/FAA/AR-03/57 (2003).

34. Agüera, N.D., Tornello, M.E., and Frau, C.D. "Structural response of unreinforced masonry walls", *Journal of Civil Engineering and Architecture*, **10**, pp. 219–231 (2016).

35. Arias, A., Rodríguez-Martínez, J.A., and Rusinek, A. "Numerical simulations of impact behavior of thin steel

plates subjected to cylindrical, conical and hemispherical non-deformable projectiles", *Engineering Fracture Mechanics*, **75**, pp. 1635–1656 (2008).

36. Wei, Z.G., Yu, J.L., and Batra, R.C. "Dynamic buckling of thin cylindrical shells under axial impact", *International Journal of Impact Engineering*, **32**, pp. 575–592 (2005).
37. Szuladzinski, G., *Formulas for Mechanical and Structural Shock and Impact*, CRC Press (2009).
38. Moxley, R.E., Adley, M.D., and Rohani, B. "Impact of thin-walled projectiles with concrete targets", *Shock and Vibration*, **2**(5), pp. 355–364 (1995).

Biographies

Morteza Taheri is currently a PhD student at the Department of Mechanical Engineering, Islamic Azad University, Damavand Branch. He obtained his MSc degree from Isfahan University of Technology and his BSc degree from Islamic Azad University, Najafabad Branch, all in Mechanical Engineering. He is working as a Mechanical Engineer in an Iranian industrial research company. His research interests are in the fields of impact mechanics, nose design, and design of thin wall structures.

Omid Kavianipour is currently an Assistant Professor at the Department of Mechanical Engineering, Islamic Azad University, Damavand Branch. He received his PhD degree from Iran University of Science and Technology, Tehran in 2014, in Mechanical Engineering, MSc degree from K.N. Toosi University, Tehran in 2008, in Aerospace Engineering, and BSc degree from Islamic Azad University Science and Research Campus, Tehran in 2005, in Mechanical Engineering. His research interests are in vibration, control, automation, and mechanism design. He has several papers in journals and conferences.